PROCEEDINGS, Thirty-Seventh Workshop on Geothermal Reservoir Engineering
Stanford University, Stanford, California, January 30 - February 1, 2012
SGP-TR-194

IMPACT OF FLUVIAL SEDIMENTARY HETEROGENEITIES ON HEAT TRANSFER AT A GEOTHERMAL DOUBLET SCALE

Virginie Hamm and Simon Lopez

BRGM
3, Avenue Claude Guillemin
Orleans, 45000, France
e-mail: v.hamm@brgm.fr

ABSTRACT

Deep Triassic aquifers of the Paris sedimentary basin are located in clastic series which are mainly composed of fluvial deposits. They lie between 2000 and 3000 m depth and their temperature can reach 120°C in some areas. There were few attempts (3) at geothermal exploitation in the early 80's but none of them was really successful (exploitation was performed during one year on one site but injection pump failure and well damage lead to abandonment). In the context of the renewal of geothermal exploration and development in the Paris basin several new projects are now considered. As a preliminary study of the specificities of Triassic aquifers, we investigated the impact of sedimentary heterogeneities of such environments on the hydrodynamic and thermal behaviour of a geothermal doublet (1 producer well and 1 injector well). Two orientations of wells were simulated: vertical wells and horizontal wells. The main objectives are i) to study the impact of these heterogeneities and of the type of exploitation (vertical or horizontal wells) on the shape of the cold plume developing around the injector and on the thermal breakthrough time, and ii) to explore a relationship between a heterogeneous model of permeability and a more simplistic model that could potentially describe heat transfer processes at the doublet scale.

For the numerical simulations we used a 3D numerical block obtained with a process-based model of fluvial sedimentary deposits (Flumy model developed by Mines Paristech). This synthetic block is 5 km long, 4 km wide and 50 m thick. It is composed of 200 cells in x and z directions for 160 cells in y direction (6.400.000 cells). For numerical limitation, it was upscaled to 100 cells in x and z directions and 80 cells in y direction (800.000 cells). Doublet simulations were performed considering two cases: the doublet is parallel to the main channels; or the doublet is perpendicular to the main channels.

The simulation results were then compared to those obtained with a simple hydrogeological model with the heterogeneous model being replaced by a 2 layers model which cumulates sand bodies and clay bodies. For each simulation a passive tracer was added to the cold injected water to compare the geometry of the cooled part of the reservoir to the injected fluid paths.

MODEL DESCRIPTION

In this study we carried out numerical simulations to investigate the impacts of sedimentary heterogeneities on geothermal heat exploitation of fluvial aquifers of the triassic series of the Paris basin using a realistic fluvial reservoir model.

Static reservoir modeling of fluvial deposits

In the oil industry, accurate sedimentary heterogeneities description is key aspect of reservoir characterization as they may have a significant impact on dynamic processes such as water flooding and oil recovery (*e.g.* Pranter *et al.*, 2007). Static reservoir modeling most often relies on geostatistical techniques to directly reproduce the distribution of the parameters of interest (lithofacies, petrophysical properties…) based on estimations from spatial statistics and on the choice of an appropriate probabilistic model. Even if the classification may seem by way much too simple two family of methods may be distinguished: pixel based models where a continuous function is evaluated on a discrete grid and boolean methods that consist in throwing randomly discrete objects into space. As both types of methods can be used to produce conditional simulation honoring well constraint they are intensively used for practical purposes (e.g. Chilès & Delfiner, 1999).

In this study we used a static 3D numerical block representing the sedimentary architecture produced using a combined stochastic and process-based approach. This alternative method has been developed for modeling fluvial meandering channels at the hydrocarbon-reservoir scale (Lopez *et al.*, 2008 ; Lopez, 2003). It is especially suited for exploration phases when data are relatively scarce. In this context, deterministic equations from the hydraulic literature are used to palliate the relative lack of subsurface data. As it mimics sedimentary processes this method produces numerical blocks that are geologically constituent and quite realistic. The different elements have been implemented taking into account physical results and case study reports. The three-dimensional evolution of the channel stems from equations developed in hydraulic studies and proven to generate realistic two dimensional shapes. The model allows for the generation of the different elements of fluvial deposits: point bars, crevasse splays, overbank alluvium, sand and mud plugs (Lopez *et al.*, 2008). This method has been implemented in the Flumy[1] software and has been successfully tested by several oil companies.

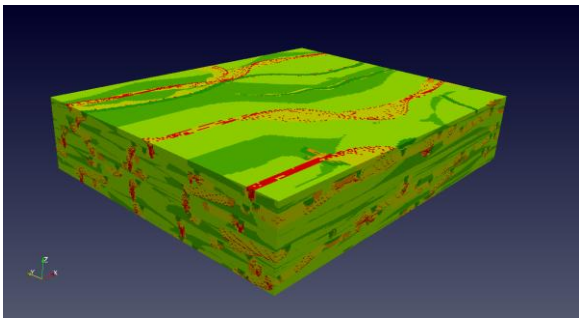

Figure 1: 3D lithofacies block from the Flumy model. (6 million cells) There are 9 different lithofacies (cf. table 1). Relatively permeable sandy facies are represented in red and yellow (channel lags, sand plugs, point bars) whereas more impervious facies are in shades of green (overbank deposits, alluvial plain) (20x vertical exaggeration)

Description of the 3D heterogeneous block

In this study we used a numerical block produced with the Flumy software which is 5 km long, 4 km large, and 50 m high. The reservoir was generated using a 100 m width channel and simulation parameters were tuned to obtain a "ribbon" type reservoir[2] (named "ribbon" because of permeable sand bodies that are relatively narrow and disconnected). Nine lithofacies are used to represent the sedimentary deposits and fill a regular grid with a 25 m horizontal spacing and a 25 cm vertical spacing which makes 6 million cells. A 3D view of the lithofacies block is shown in figure *1* and table *1* lists the nine lithofacies name.

In order to represent the deep series of the Paris basin petrophysical values (porosity, horizontal and vertical permeabilities) have been assigned to each lithofacies using data from the literature on the Chaunoy oil field (Eschard *et al.*, 1998). Thermal conductivities have been chosen among usual values for sedimentary deposits and some work could be done to further investigate the impact of the variability of these parameters. Table *1* lists petrophysical properties values that have been assigned to each lithofacies (*rocktyping*).

Table 1: Lithofacies and associated petrophysical values

lithofacies	porosity (%)	horizontal permeability (mD)	vertical permeability (mD)	thermal conductivity (W/m/°C)
channel lag	15	400	400	4.5
sand plug	10	50	1	4.5
point bar	8	400	5	4.5
crevasse splay I	12	80	80	2.5
crevasse splay II channels	8	50	1	3
crevasse splay II	20	1	0.1	2.5
mud plug	20	0.1	0.01	1.5
overbank alluvium	20	0.2	0.02	1.5
levee	12	1	0.1	2

[1] More information about the Flumy software and free evaluation versions may be downloaded at : http://www.geosciences.mines-paristech.fr/en/organization/presentation-of-the-group-2/main-projects/flumy-turmy

[2] A similar numerical block may be downloaded from the Flumy website (cf. note 1).

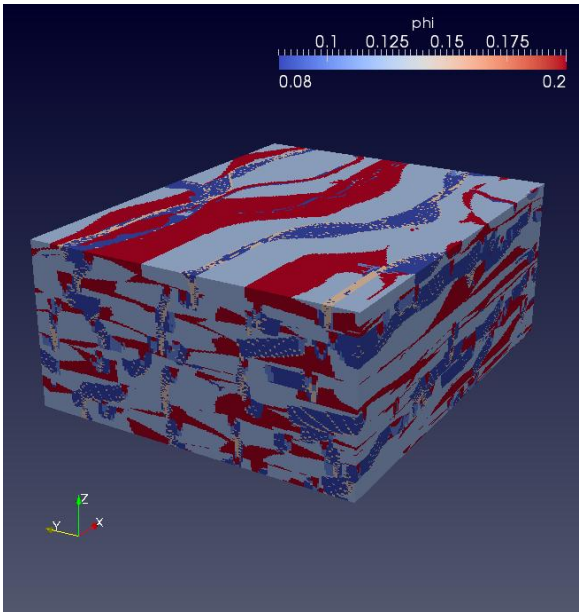

Figure 2: Porosity values of the original block (6 million cells block with porosity values given by table *1*) *(40x vertical exaggeration)*

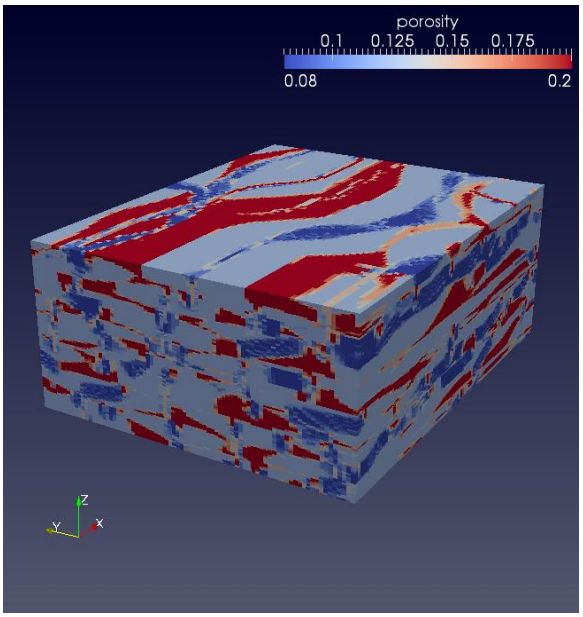

Figure 3: Porosity values of the upscaled 800,000 cells block *(40x vertical exaggeration)*

As the 6 million cells grid was much too big to perform hydrodynamic and thermal simulation with BRGM sequential simulator Marthe, simple upscaling techniques were used to produce a coarser 800,000 cells grid with a 50 m horizontal spacing and a 0.5 m vertical spacing. The formula used to upscale permeabilities and thermal conductivites in a given direction is the one from Le Loc'h, 1987 cited by Renard *et al.*, 2000. Le Loc'h, 1987 showed that the equivalent permeability for a uniform flow in a given direction has an upper bound which is the harmonic mean of the arithmetic means of the local permeabilities calculated over each slice of cells perpendicular to the given direction and a lower bound which is the arithmetic mean of the harmonic means of the local permeabilities, calculated on each line of cells parallel to the given direction. She proposed to take the geometric average of these bounds as the upscaled value, which writes:

$$K^x = \sqrt{\left[\mu_h^x\left(\mu_a^y\left(\mu_a^z\right)\right)\right]\left[\mu_a^y\left(\mu_a^z\left(\mu_h^x\right)\right)\right]} \quad (1)$$

Where K^x is the upscaled value in the x direction, μ_a^x stands for the arithmetic mean in the x direction and μ_h^x denotes the harmonic mean in the x direction. Porosity was upscaled using a harmonic mean. Figures *2* and *3* show the comparison between the original and upscaled porosity blocks.

MODELING OF A GEOTHERMAL DOUBLET EXPLOITATION

The doublet exploitation consists of a closed loop: fluid is pumped at the production well and after cooling through a heat exchanger is then fully reinjected in the reservoir. Two critical parameters define the lifetime of a geothermal doublet: the thermal breakthrough time and the extent of the cold plume. The former parameter indicates the time from which the production temperature is decreasing due to a variable mixture with time of the reservoir original fluid and of the cold injected water. The latter parameter indicates the volume of the aquifer which is impacted by the cold injection. These two parameters are crucial for geothermal exploitation, because a premature production temperature cooling will affect the profitability of the exploitation and a good knowledge of the development of cold water bodies in the aquifer is a key aspect of its sustainable exploitation.

Wells location and properties

Two set of wells were considered: vertical wells and horizontal wells. For each set of wells two orientations of the double axis were studied: parallel to main permeable bodies represented by the sand channels (Ox direction) or perpendicular to the channel axis (Oy direction). Wells were simply simulated by assigning a very high permeability value (10^{-9} m^2) to grid cells along the well path. Vertical wells were located 1 km apart and were considered to cross entirely the simulation block. Horizontal wells were 750 m long and 750 m apart.

They were located on the same horizontal level, in the middle of the block (25 m high in the Oz direction). For every studied case the doublet was centered on the simulation block.

Simulation tool

Dynamic modeling was performed using the MARTHE software package developed by BRGM (Thiéry, 1990). MARTHE is a finite-difference hydrodynamic package that processes three-dimensional flow in both saturated and unsaturated condition and can handle heat transport taken into account the temperature dependence of density and viscosity.

The heat loss by conduction to surrounding impervious formations was not taken into account. This is the reason why temperature production declines are relatively high and would probably be much less for a real case study (Lopez et al, 2010).

Comparison between wells orientation (vertical or horizontal)

Table 2: Production temperature decline

	Wells position			
	Parallel to channels		Perpendicular to channels	
	Wells orientation		Wells orientation	
	vertical	horizontal	vertical	horizontal
ΔT (°C) after 5 years	0.78	1.12	0	0
ΔT (°C) after 10 years	6.86	4.17	0	0
ΔT (°C) after 20 years	15.19	9.51	0.01	0
ΔT (°C) after 30 years	19	12.77	0.16	0.02

In this paragraph, we compare the production temperature evolution and the plume extension between vertical and horizontal wells simulations. Two configurations are studied: (1) wells are parallel to the main channels direction and (2) wells are positioned perpendicularly to the main channels direction. The conditions for the numerical simulations are a constant flow rate of 200 m^3/h and a reinjected fluid temperature of 40 °C. The initial fluid temperature was set to 90°C which is the average temperature of the Trias formation.

Table *2* summarizes the production temperature decline with time after 5, 10, 20 and 30 years of geothermal exploitation (typical duration of a doublet operating permit).

Figure *4* shows the temperature evolution in the case of wells positioned in the direction of the channels (x direction) where a temperature decline is observed.

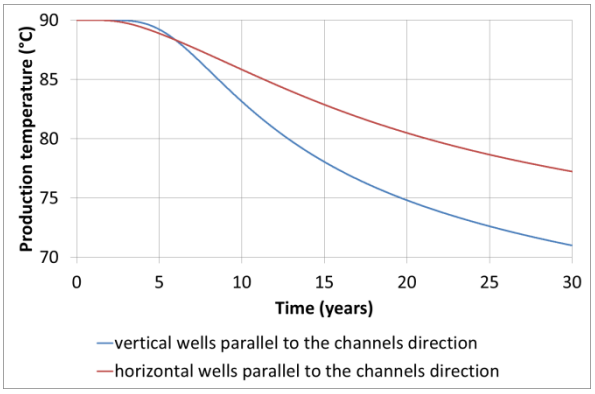

Figure 4: Evolution of the production temperature during exploitation for horizontal wells

The comparison between the two modes of exploitation (vertical or horizontal wells) shows a clear difference in the thermal evolution. ***In the case of wells parallel to the channels***, (columns 1&2 of table *2* and figure *4*), the production temperature decline is first observed for horizontal wells. From 6 years of simulation, the temperature drop becomes stronger for vertical wells. The difference between the production temperature curves is growing with time and the production temperature is 6.2 °C colder for vertical wells than for horizontal wells after 30 years of doublet exploitation. The shorter distance between horizontals wells (750 m instead of 1 km for vertical wells) induces shorter path lines between the closest extremities of the horizontal wells but also longer path lines because of the horizontality of the wells (each of 750 m long). Nevertheless, as there are relatively more longer path lines than shorter ones, the production temperature decline will start earlier but will be slower. This shows that horizontal wells are particularly interesting for geothermal purpose because the production temperature evolution is more gradual. ***In the case of wells perpendicular to the channels***, (columns 3&4 of table *2*), the numerical simulations for the two wells configurations do not show any perceptible decline after 30 years of exploitation. In the case of vertical wells, the flow rate of 200 m^3/h couldn't be simulated (numerical divergence) because of too low permeability. Thus for this particular simulation, a flow rate of 100 m^3/h was used. Those simulations show the importance of fluvial sedimentary heterogeneities on wells position

and consequently on the production temperature evolution. Thus, if the heterogeneities are well known, it is a good opportunity (mainly for horizontal wells) to set up wells perpendicular to the principal direction of channels. In this case, the duration of exploitation can be easily extended under the condition that the wells remain in good state enough. For vertical wells, as shown by numerical simulation, there could be a problem of injectivity because the risk is greater not to intersect permeable facies when drilling and to be consequently unable to pump at a flow rate compliant with an industrial project economics.

Figures *5* to *8* show for each wells configuration the geometry of the cold plume around the injector after 10 years of thermal exploitation. As mentioned above, the extension of the cold plume is not the same in the cases where the wells are perpendicular or parallel to the direction of the main permeable bodies. If we compare the cold plume extension for horizontal wells (same simulation conditions), we observe that unlike the first configuration where the well doublet axis is parallel to Ox (fig. *6*), in the second case where the doublet axis is parallel to Oy (fig. *8*), the cold plume is developing preferentially in the channel direction, and therefore the cold plume will not reach the production well.

It is worth noting that recently, Ungemach *et al.* (2011) stresses the potential benefit of using horizontal wells for the geothermal exploitation of the carbonate Dogger aquifer of the Paris basin.

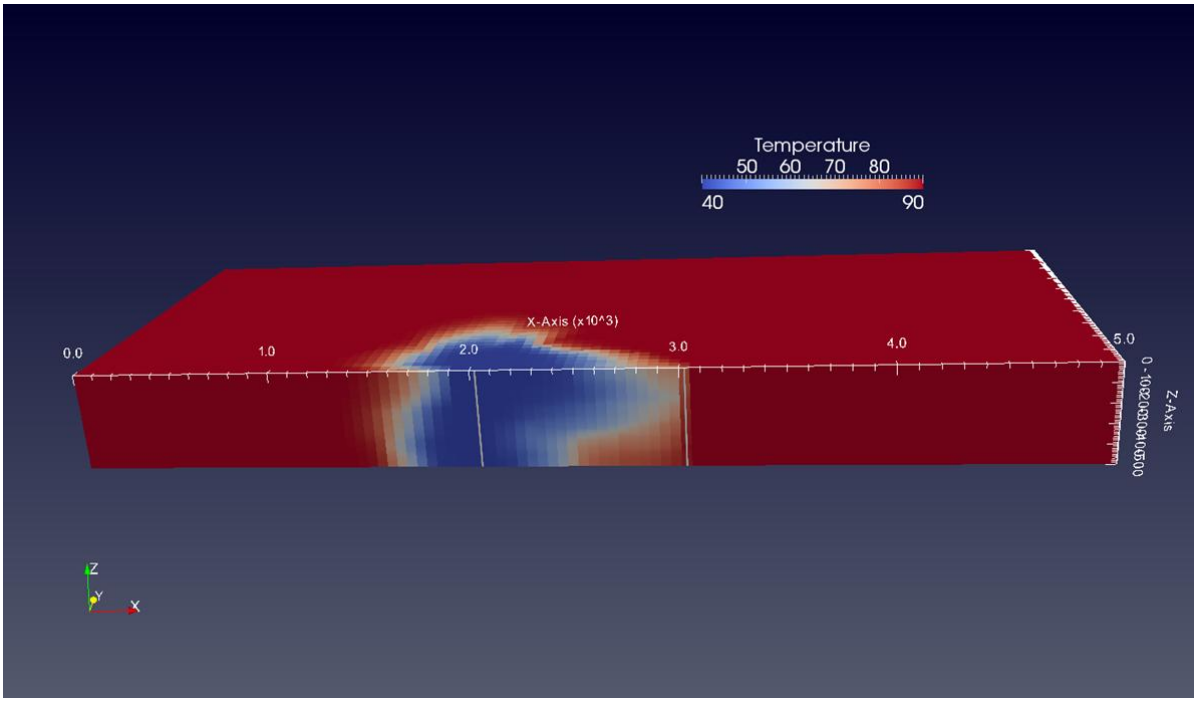

Figure 5: Cold plume extension after 10 years of geothermal exploitation (vertical wells positioned in parallel to channels, x direction).

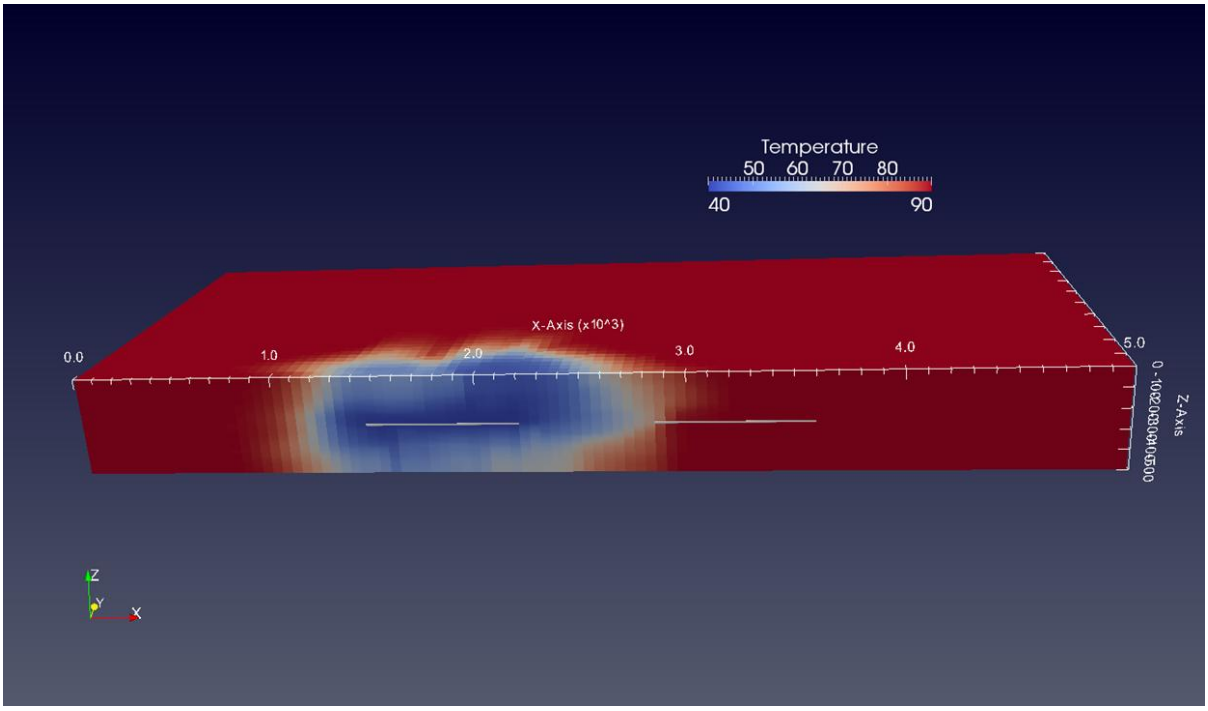

Figure 6: Cold plume extension after 10 years of geothermal exploitation (horizontal wells positioned in parallel to channels, x direction)

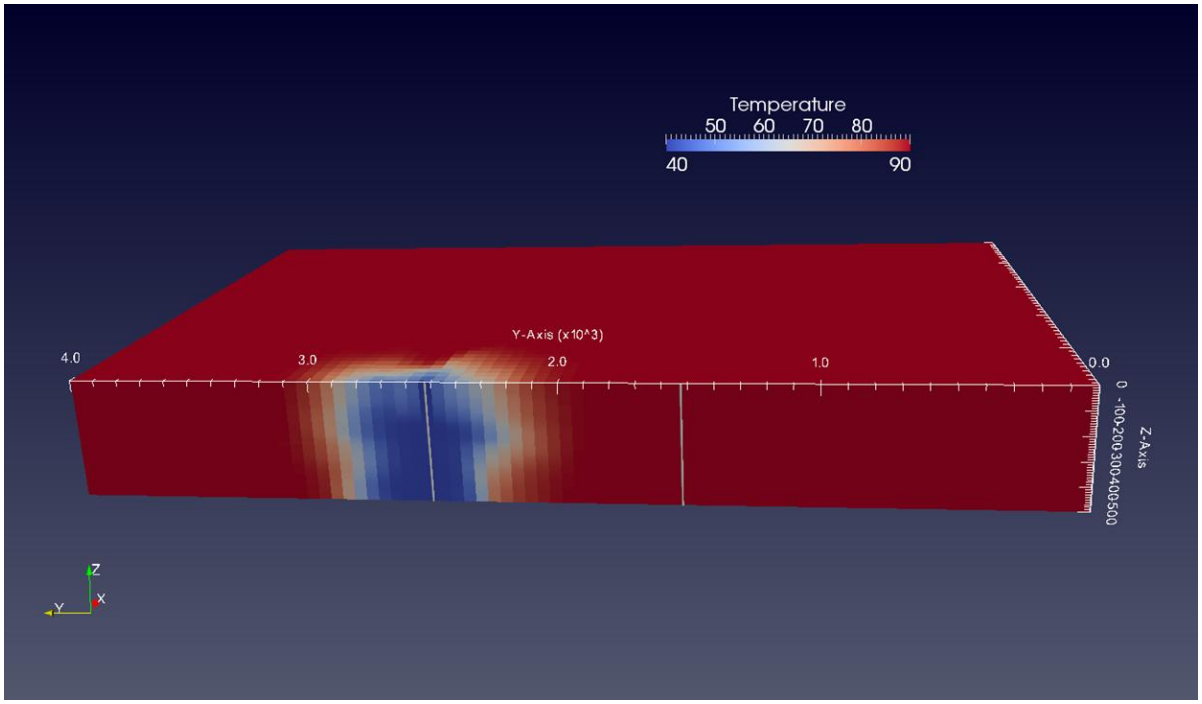

Figure 7: Cold plume extension after 10 years of geothermal exploitation (vertical wells positioned perpendicularly to channels, y direction).

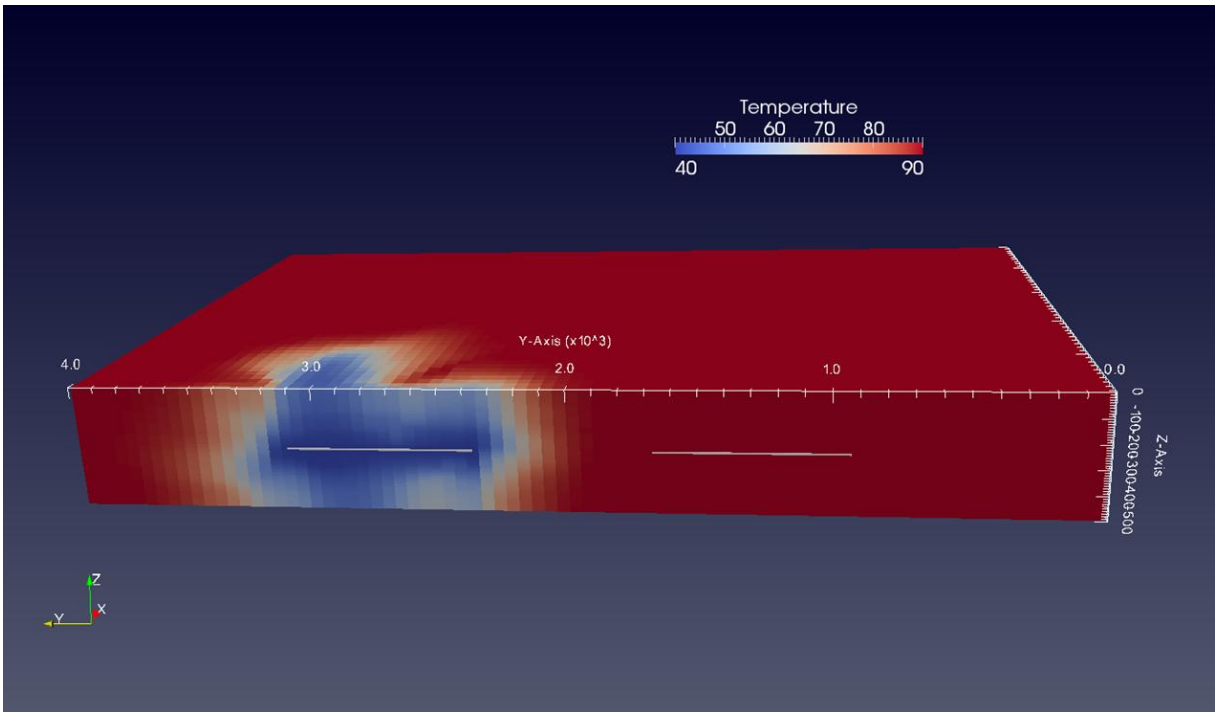

Figure 8: Cold plume extension after 10 years of geothermal exploitation (horizontal wells positioned perpendicularly to channels, y direction).

Comparison with a simulation involving density effect for horizontal wells

In this paragraph, we study the effect of density variation with temperature in the case of horizontal wells parallel to channels. The other simulation conditions remain unchanged.

Table *3*, shows the cooling at the production well after a period of 5, 10, 20 and 30 years of geothermal exploitation. Figure *9*, shows the two production temperature curves for each simulation.

Table 3: Production temperature decline

	Horizontal wells - fixed density	Horizontal wells - variable density
ΔT (°C) after 5 years	1.12	0.6
ΔT (°C) after 10 years	4.17	2.42
ΔT (°C) after 20 years	9.51	6.1
ΔT (°C) after 30 years	12.77	8.84

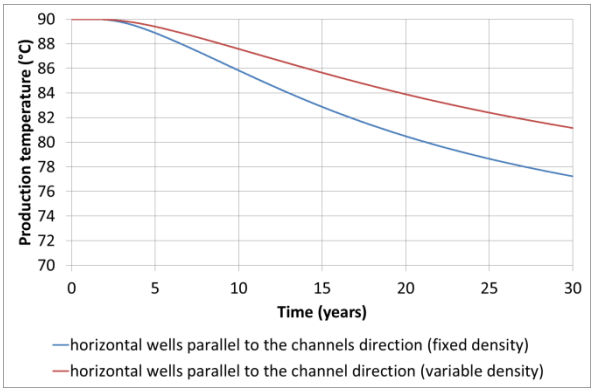

Figure 9: Comparison of the production temperature for horizontal wells between the simulation with and without density effect.

This simulation shows that density effect induces a delay in the production temperature drop. This trend could be amplified on purpose to delay thermal breakthrough if the location of wells is well designed by setting the injection well deeper than the production well (same depth for this theoretical study).

Comparison between the cold plume geometry and a tracer injection

In this second set of simulations, we compare the cold plume extension to the pathways of an injected tracer. Thus, the 40°C injected fluid is "numerically dyed" using a conservative tracer concentration of 1 g/l. The objective is to assess the impact of the heterogeneities on the displacement of the cold front compared with the displacement of the injected fluid. Figure *10*, shows the production concentration curves evolution in time for each case (vertical or horizontal wells and parallel or perpendicular to channels)

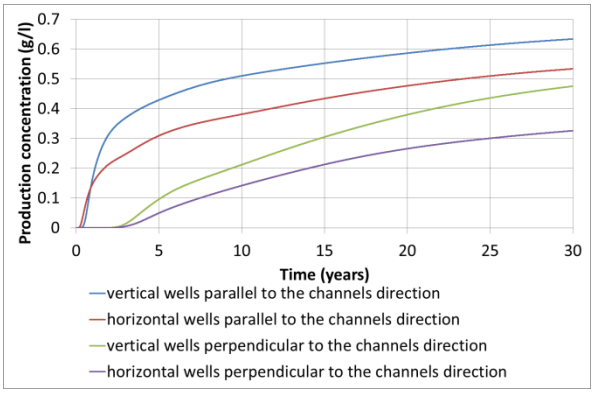

Figure 10: Production concentration curves

Tracer arrival is observed for every simulation, even for horizontal wells set perpendicular to the channels direction, contrary to what could suggest the production temperature that remained relatively constant in that case. Nevertheless, the tracer breakthrough time is much longer.

.

Figures *11* to *14* show the isocontours of the invaded areas by both the cold injected water and the injected tracer. The red arrow symbolizes the position of the production well. We observe a clear difference between the volume of aquifer disturbed by the cold injection and the volume invaded by the injected tracer. If we try to compare the respective shapes of the cold plume and the tracer plume, the temperature isocontours are somewhat close to a distorted cylinder. On the contrary, the tracer isocontours are much more impacted by the heterogeneities with the fluid following preferential paths corresponding to high permeability bodies.

Figures *15* and *16* show respectively for vertical and horizontal wells, a cross section of the reservoir between wells. From top to bottom, we can see the horizontal permeability field (orange: high permeability, blue: low permeability), the temperature and concentration fields after 1 and 10 years of injection (orange: temperature of 90°C or tracer concentration of 1g/l, blue: temperature of 40°C and tracer concentration of 0 g/l). This illustrates that the fluid is preferentially following along high permeability paths. The velocity of the tracer is always greater than of cold front velocity (De Marsily, 1986). For block porosity ranging from 0,08 to 0,2, the tracer velocity is 3 to 6 times higher than the thermal velocity. Furthermore, as the heat diffusion is 10^3 to 10^5 greater than the tracer diffusion, the thermal front tends to homogenize further away from wells where velocities are smaller, which makes that its shape is much less contrasted than the tracer front.

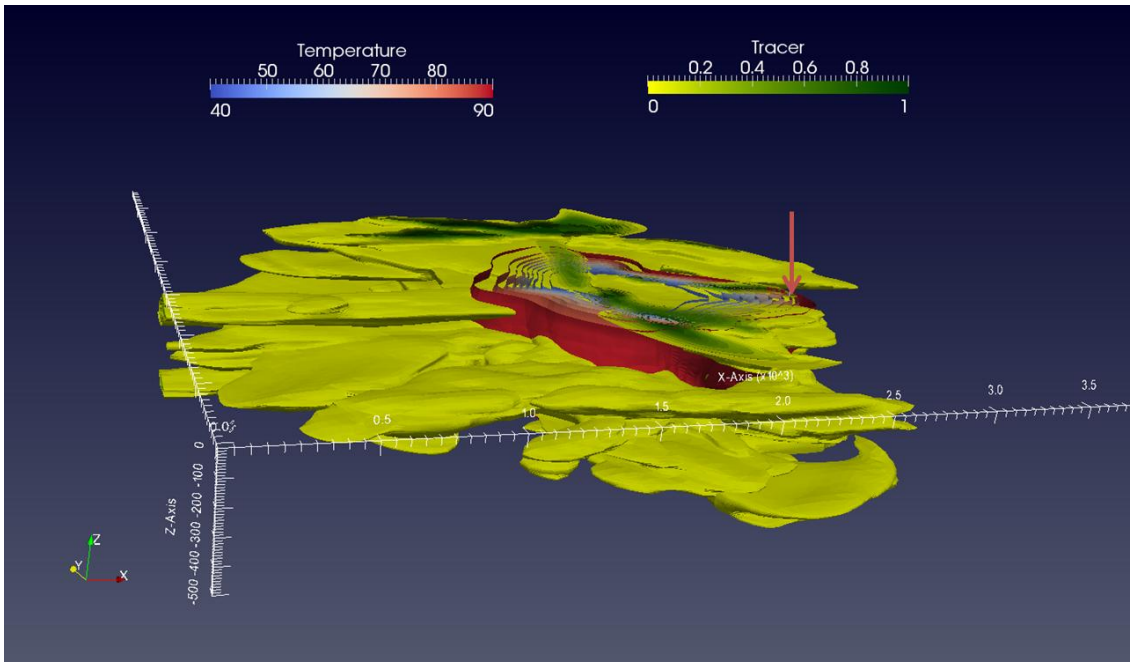

Figure 11: Temperature and tracer isocontours after 10 years of exploitation (vertical wells oriented according x direction).

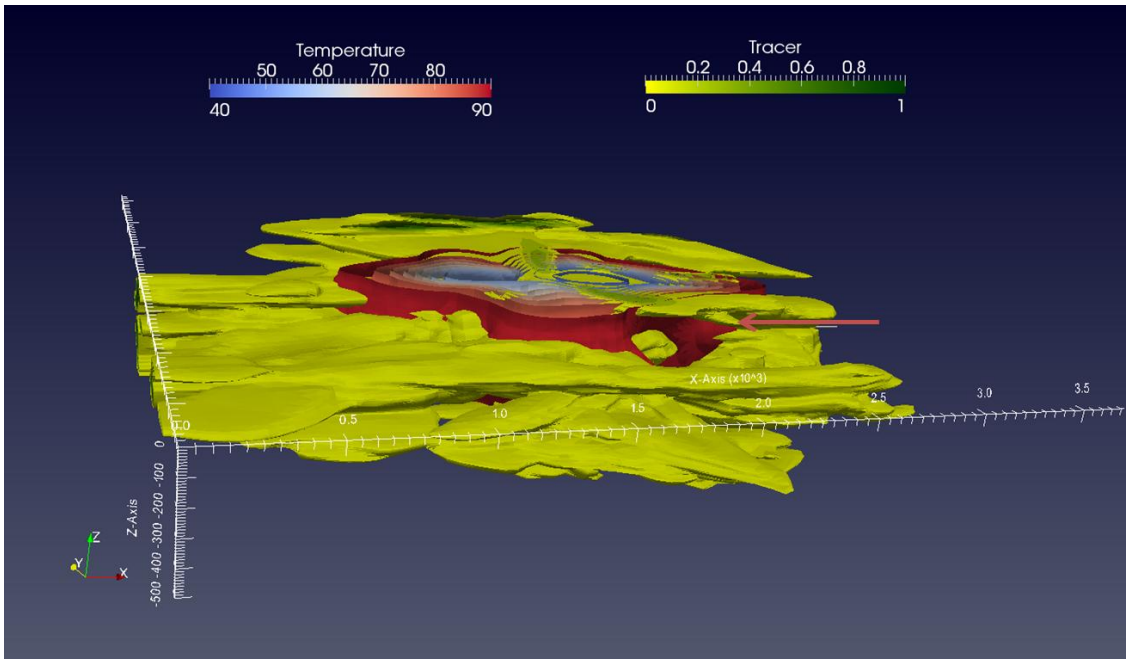

Figure 12: Temperature and tracer isocontours after 10 years of exploitation (horizontal wells oriented according x direction).

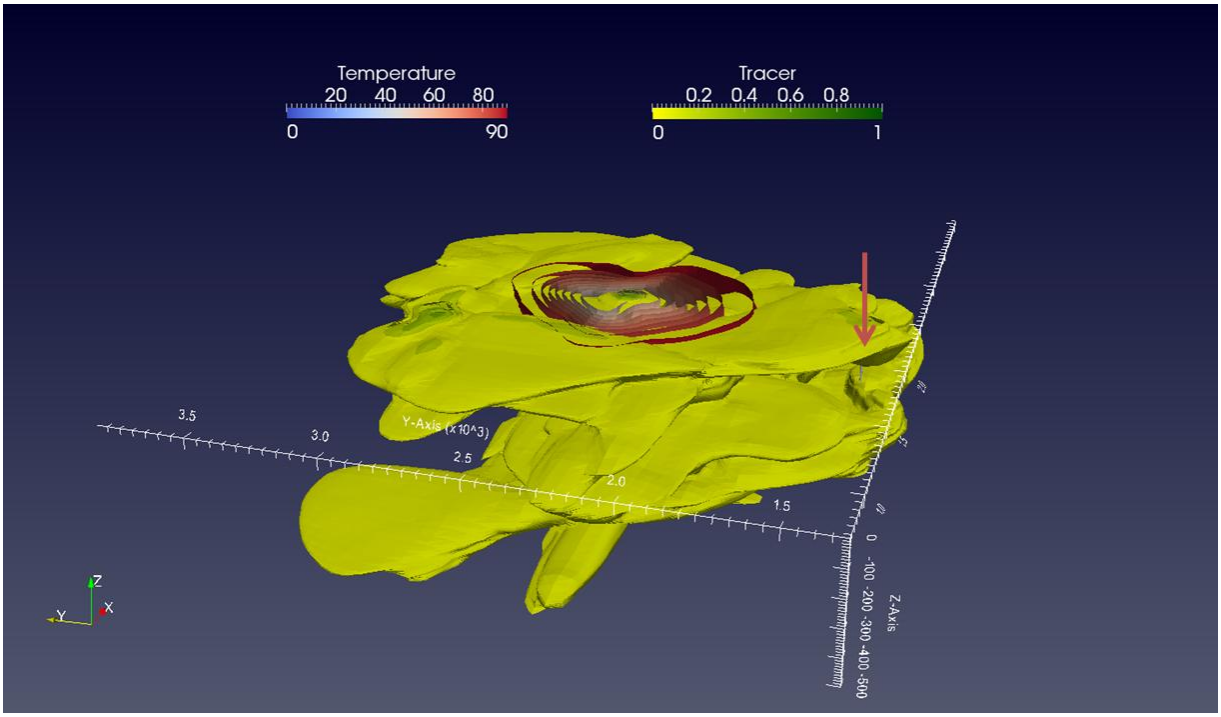

Figure 13: Temperature and tracer isocontours after 10 years of exploitation (vertical wells oriented according y direction).

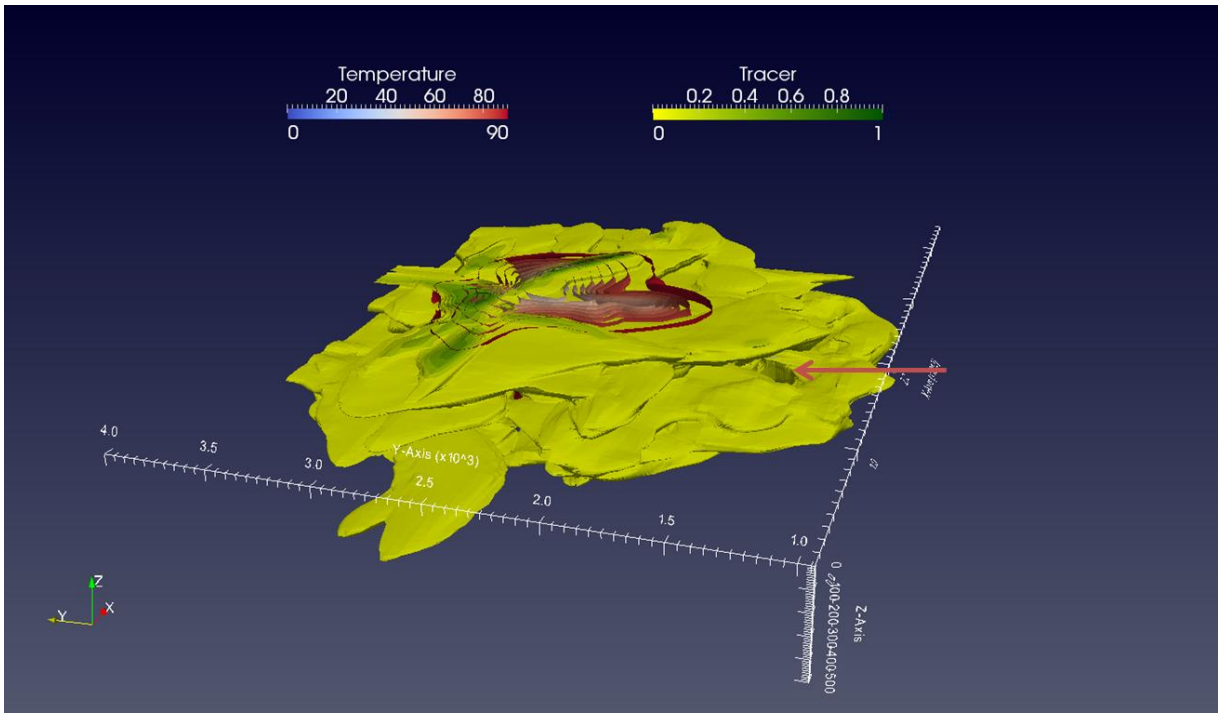

Figure 14: Temperature and tracer isocontours after 10 years of exploitation (horizontal wells oriented according y direction).

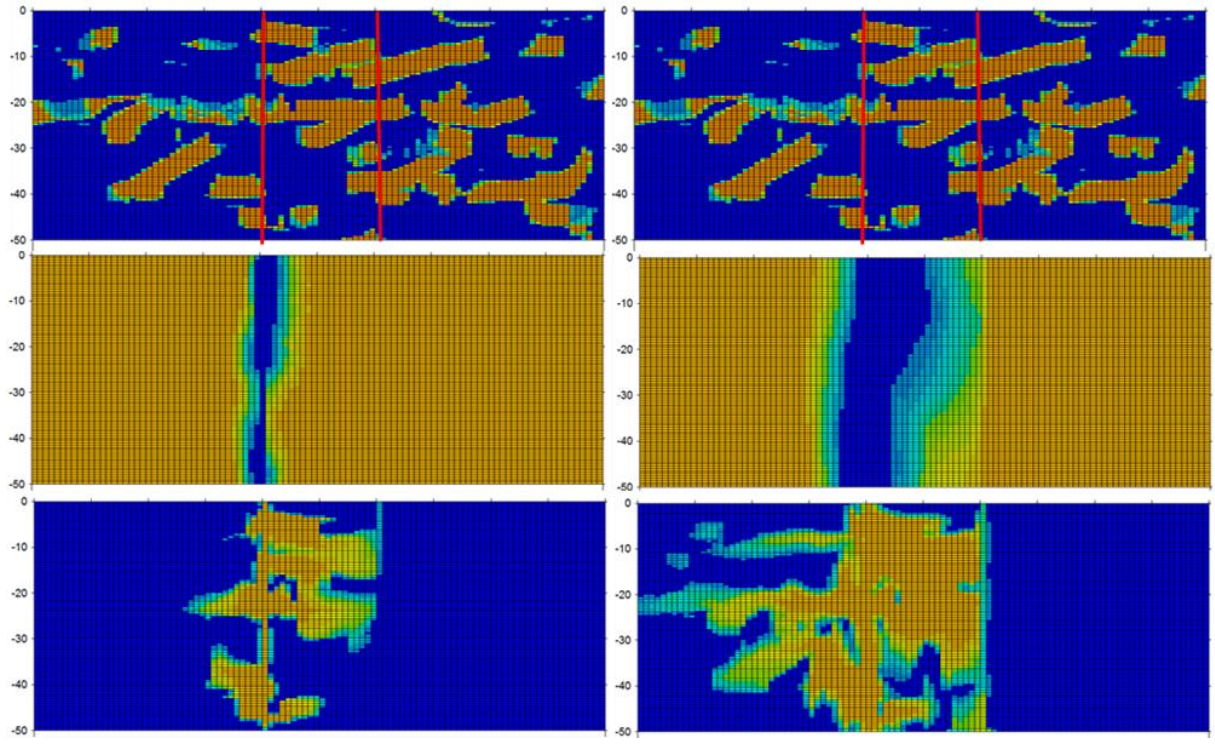

Figure 15: From top to bottom: horizontal permeability field and position of vertical wells (red lines), temperature and tracer fields after 1 year (left) and 10 years (right)

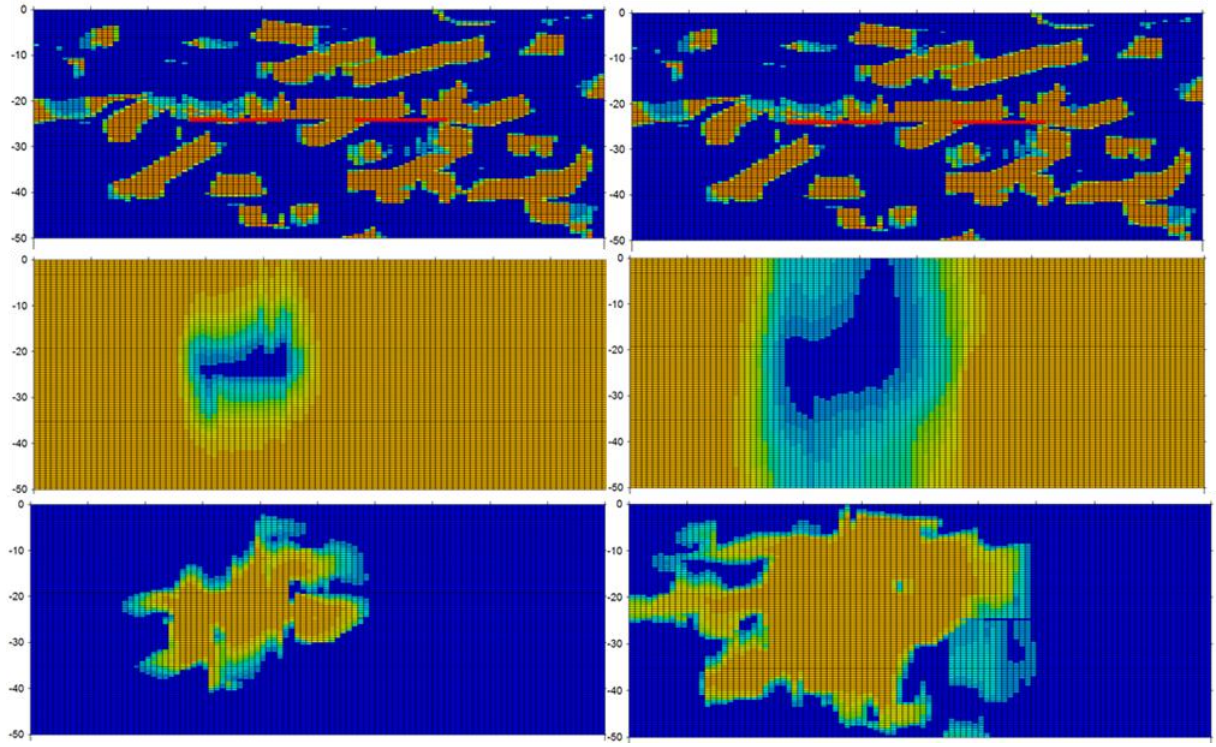

Figure 16: From top to bottom: horizontal permeability field and position of horizontal wells (red lines), temperature and tracer fields after 1 year (left) and 10 years (right)

COMPARISON BETWEEN THE HETEROGENEOUS MODEL AND A SIMPLIFIED HOMOGENOUS MODEL

In the previous paragraph, we discussed about the fact that heterogeneities can lead to channeling along specific paths and lead to short first tracer arrival times. By contrast, the thermal front seems to be less impacted by channeling because the fluid is heated in contact with the rock as it is moving. Here we propose a simple method to replace the heterogeneous model, in the case of wells set in the channels direction, by an alternative homogeneous model that could describe well enough heat transfer processes at this scale.

Methodology used

The method used consists in replacing the three-dimensional heterogeneous block characterized by 100, 0.5 m thick subdivisions in the z direction, by a two-layer model with one layer cumulating the high permeability zones (net pay) and the second layer cumulating low permeability zones (interstrata). Figure *17* shows the distribution of permeability in each block direction (x, y and z) for the heterogeneous model. It shows that more than 60% of cells have horizontal permeability smaller than 2.10^{-15} m^2 and more than 20% of cells have horizontal permeability higher than 2.10^{-13} m^2.

In order to calculate the thickness of the potentially productive reservoir (net pay), we defined a threshold of permeability ranging from 1.10^{-14} to 4.10^{-13} m^2 and we calculated the net pay and transmissivity field for each cells (i,j) using the following equations:

$$h(i,j) = \left(\sum_{\substack{k \\ K_h(i,j,k) \geq Kmin}} 1 \right) \Delta z \quad (2)$$

$$T_h(i,j) = \left(\sum_{\substack{k \\ K_h(i,j,k) \geq K_{min}}} K_h(i,j,k) \right) . \Delta z \quad (3)$$

Where:

- $h(i,j)$ is the productive reservoir thickness or net pay (m)
- $K_h(i,j,k)$ is the horizontal permeability of cell (i,j,k) (m^2)
- K_{min} is the permeability threshold (m^2)
- Δz is the cell thickness in z direction (m)
- $T_h(i,j)$ is the horizontal transmissivity of cell (i,j) (m^3)

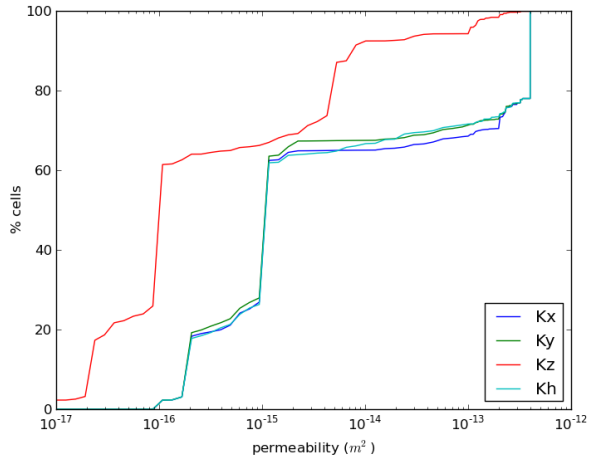

Figure 17: Distribution of permeability (m^2) in the heterogeneous block

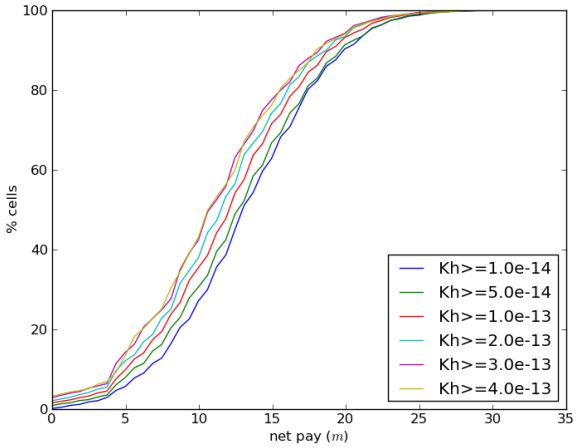

Figure 18: Distribution of the net pay (m) according to the permeability threshold

Figure *18* shows the distribution of the two-layer model productive thickness according to the permeability threshold used. The distribution of the productive thickness is similar for each threshold tested. Finally for the two-layer model construction, we kept a permeability threshold of K_{min}=5.10^{-14} m^2.

Figure *19* shows the 3D distribution of cells that are above this threshold. This figure illustrates the intricate patterns of connectivity paths between permeable bodies. Figures *20* and *21* show respectively the two-dimensional distribution of the net pay and the transmissivity field obtained by vertically averaging the previous 3D distribution.

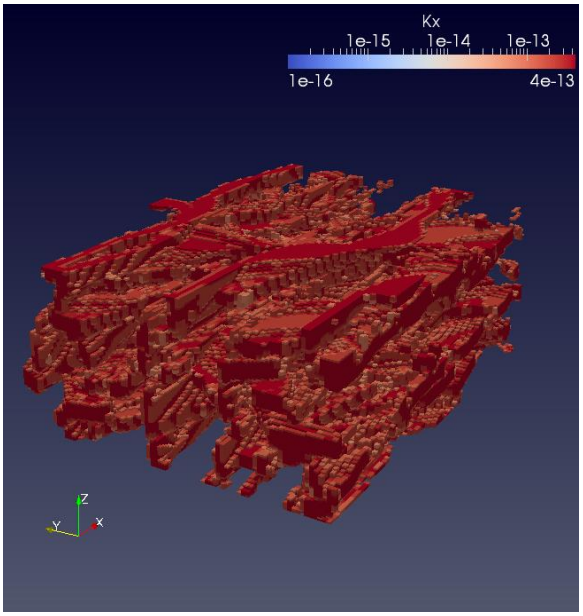

Figure 19: Cells of the coarse grid that have an horizontal permeability above the 5.10^{-14} m^2 *threshold* ($K_h \geq K_{min}=5.10^{-14}\ m^2$) *(40x vertical exaggeration)*

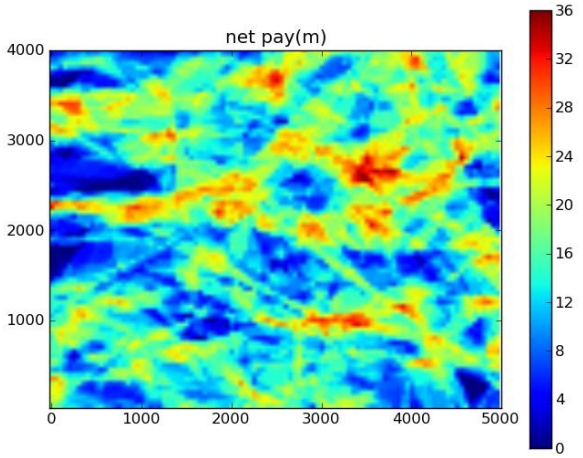

Figure 20: Productive thickness in the homogeneous model ($K_h \geq K_{min}=5.10^{-14}\ m^2$)

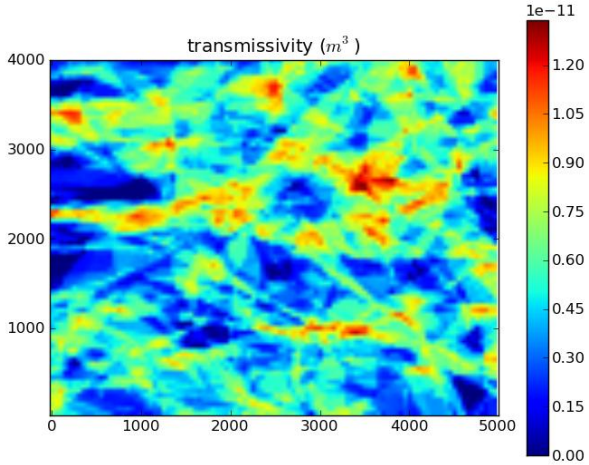

Figure 21: Productive layer transmissivity (m^3)

The thickness of the second layer representing low permeable areas, that are barriers to flow but that will transmit heat, is obtained as the difference between the total thickness (50 m) and the productive thickness. To assign a permeability to this layer we have chosen to retain the vertical permeability of the original block considering that the exchanges with the main flow that is located in the productive layer will occur perpendicularly to this layer. Moreover, as the permability values involved are relatively low this choice has no significant impact on the heat transfer between the two layers that is dominated by heat conduction. Consequently we have chosen the term of "vertical transmissivity" to note that the transmissivity of this layer was obtained using the vertical permeability. This writes using the same form as equation (3) :

$$T_z(i,j) = \left(\sum_{\substack{k \\ K_h(i,j,k)<Kmin}} Kz(i,j,k) \right) . \Delta z \qquad (4)$$

The sum being taken on the cells below the K_{min} permeability threshold (complementary set of sedimentary body depicted in figure *19*). The notations are identical to equation (3) with the vertical permeability K_z replacing the horizontal permeability K_h and T_z. replacing T_h. However, as the permeability involved are one order lower than the productive layer "real transmissivity" they will not have a great impact on the flow behavior. Figure *22* shows the interstrata transmissivity field.

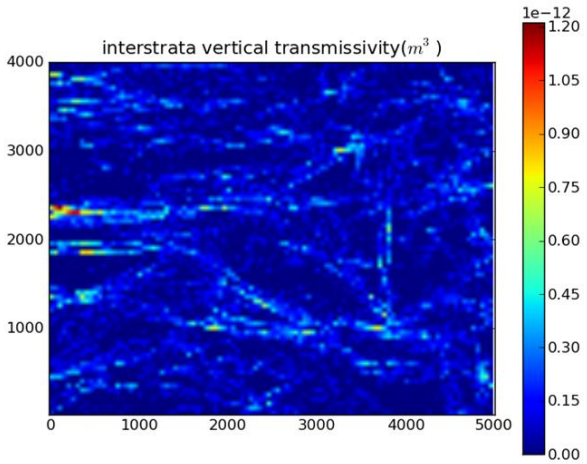

Figure 22: Interstrata transmissivity (m3)

The reservoir and interstrata porosity and thermal conductivity are obtained, by averaging the values following the vertical of each cell of the model, and according to the permeability threshold used (figures *23* and *24*)

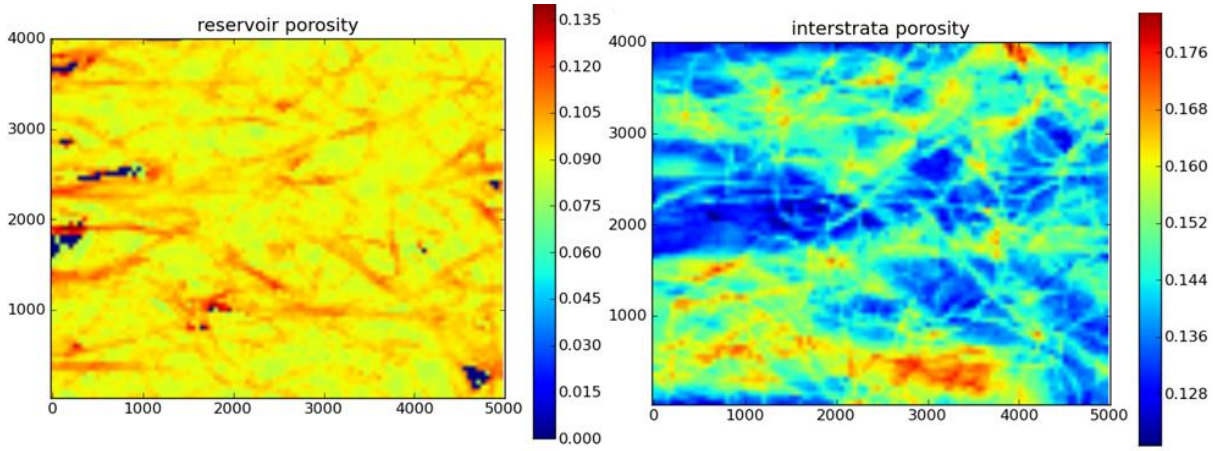

Figure 23: Reservoir and interstrata porosity

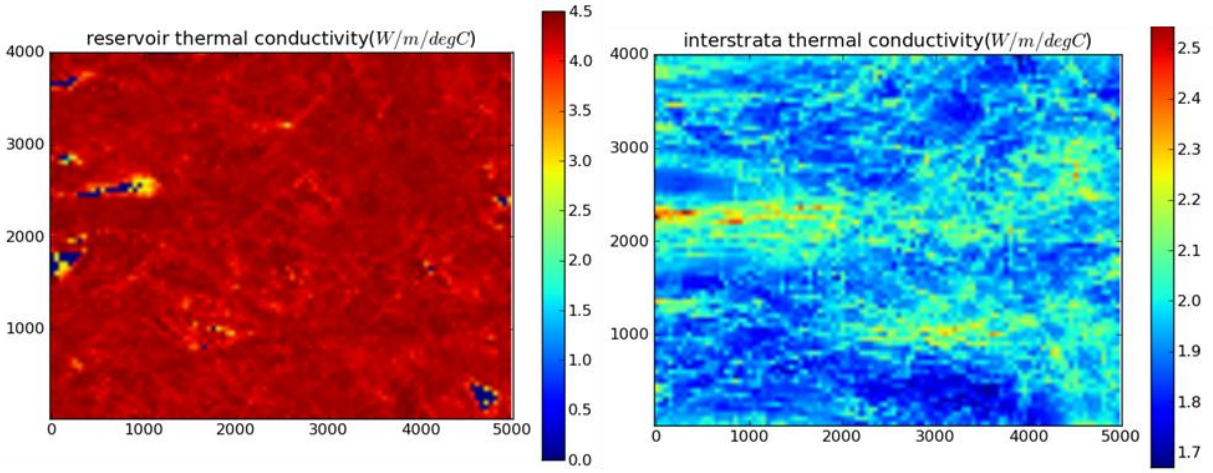

Figure 24: Reservoir and interstrata thermal conductivity (W/m/°C)

Comparison between the simplified and heterogeneous models

Temperature and tracer concentration curves

Here we compare the production temperature and the tracer restitution between the simple two-layer model and the heterogeneous block simulations. Table *4* summarizes the production fluid temperature decline after 5, 10, 20 or 30 years of exploitation for each set of simulations.

Table 4: Production temperature decline according to the type of model structure (wells are parallel to the main channel direction)

	Type of model structure			
	heterogeneous model		homogeneous model	
	Wells orientation		Wells orientation	
	vertical	horizontal	vertical	horizontal
ΔT (°C) after 5 years	0.78	1.12	4.03	4.67
ΔT (°C) after 10 years	6.86	4.17	12.49	9.75
ΔT (°C) after 20 years	15.19	9.51	16.13	12.88
ΔT (°C) after 30 years	19	12.77	18.32	14.62

Figures *25* and *26* show respectively the production temperature and tracer concentration in the case of vertical or horizontal wells and for each model structure.

The results show that the production temperature simulated by the two-layer model is rather pessimistic predicting a premature cooling at the production well. On the other hand, the first arrival time of the injected tracer is slightly later than in the heterogeneous simulations. These simulations lead to the following observations. By homogenizing the permeability on the vertical scale (cumulation of vertical cells distributed into two lithofacies), we create artificial lateral connectivity around and between wells which makes that the fluid will move through a larger volume of the domain and will reach the production well with some delay with the respect to what occurs with the connectivity of the heterogeneous model. After the tracer breakthrough time, the tracer concentration at the production well is increasing more rapidly. The production flow is consequently composed of a greater proportion of the injected fluid what will also induce premature temperature decline in this case. Our conclusion is that with such a rough homogeneous two-layer model we cannot reproduce well enough the production temperature evolution observed using the heterogeneous model.

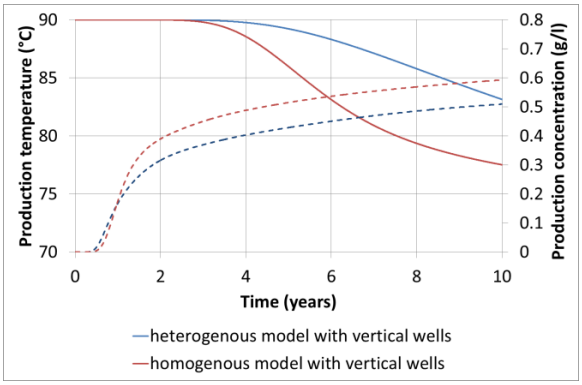

Figure 25: Comparison of the production temperature (solid lines) and tracer concentration (broken lines) between the heterogeneous model and the two-layer homogeneous model in the case of vertical wells

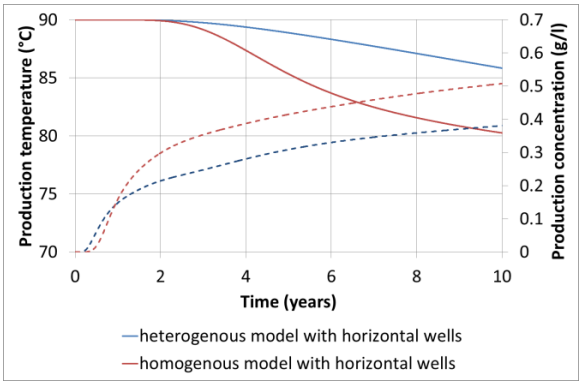

Figure 26: Comparison of the production temperature (solid lines) and tracer concentration (broken lines) between the heterogeneous model and the two-layer homogeneous model in the case of horizontal wells

Extension of the cold plume

We also compare the form of the cold plume between the two models. Figures *27* and *28* show the temperature isocontours respectively for a vertical and horizontal cold injection. We observe that in the homogeneous model, the cold front is growing mainly in the horizontal direction unlike the heterogeneous model where the cold front is developing also in the vertical direction. The shape of the cold front is like a "ship hull" with isocontours gradually warmer and closed on the bottom whereas it looks like an open distorted cylinder in the heterogeneous model. Thus those simulations show

that vertical heterogeneities have an impact on the development of the cold plume though. The two-layer model is not precise enough to reproduce the cold plume geometry.

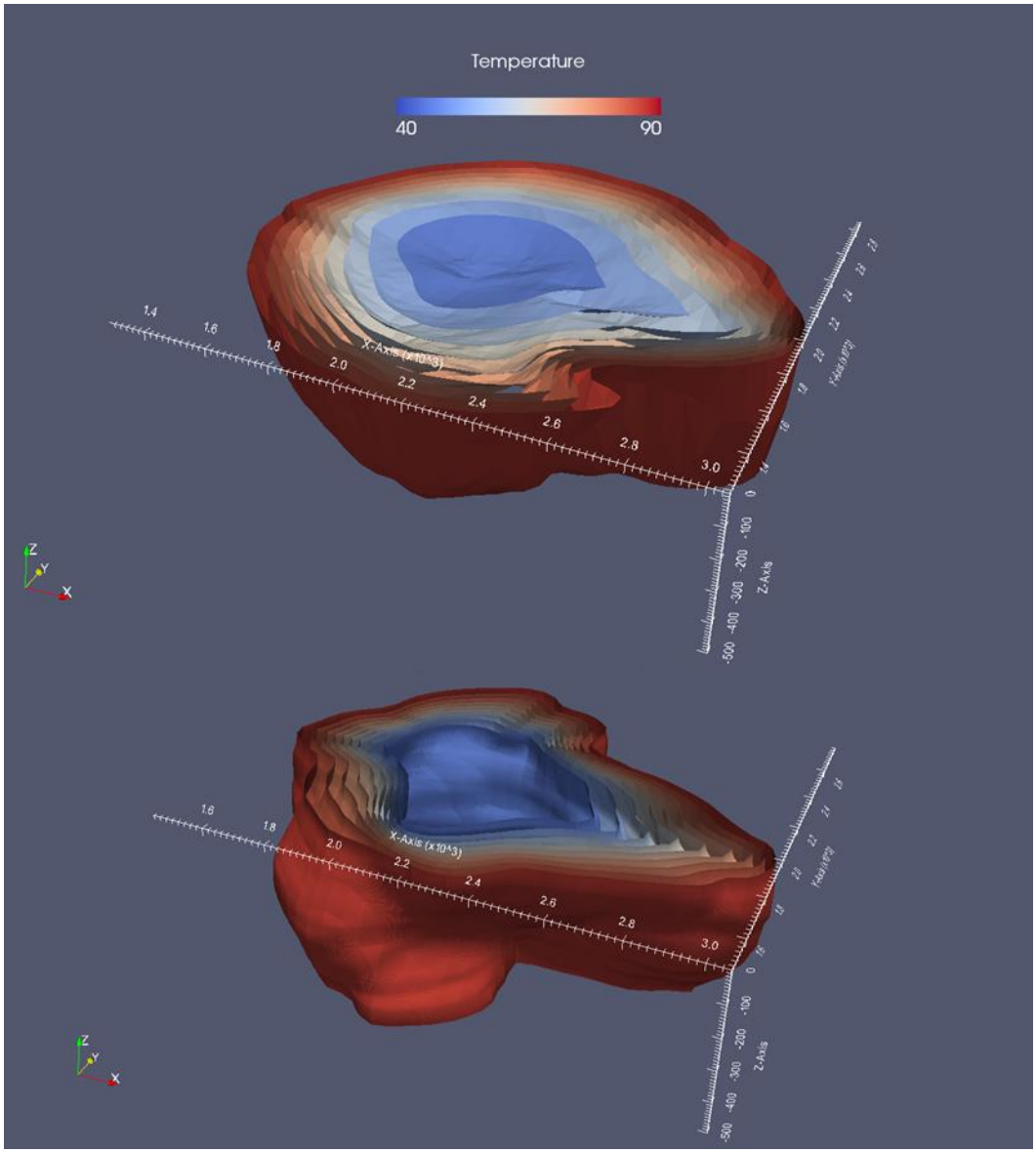

Figure 27: Comparison of the cold plume extension between the homogeneous model on the top and the heterogeneous model on the bottom. Case of vertical wells.

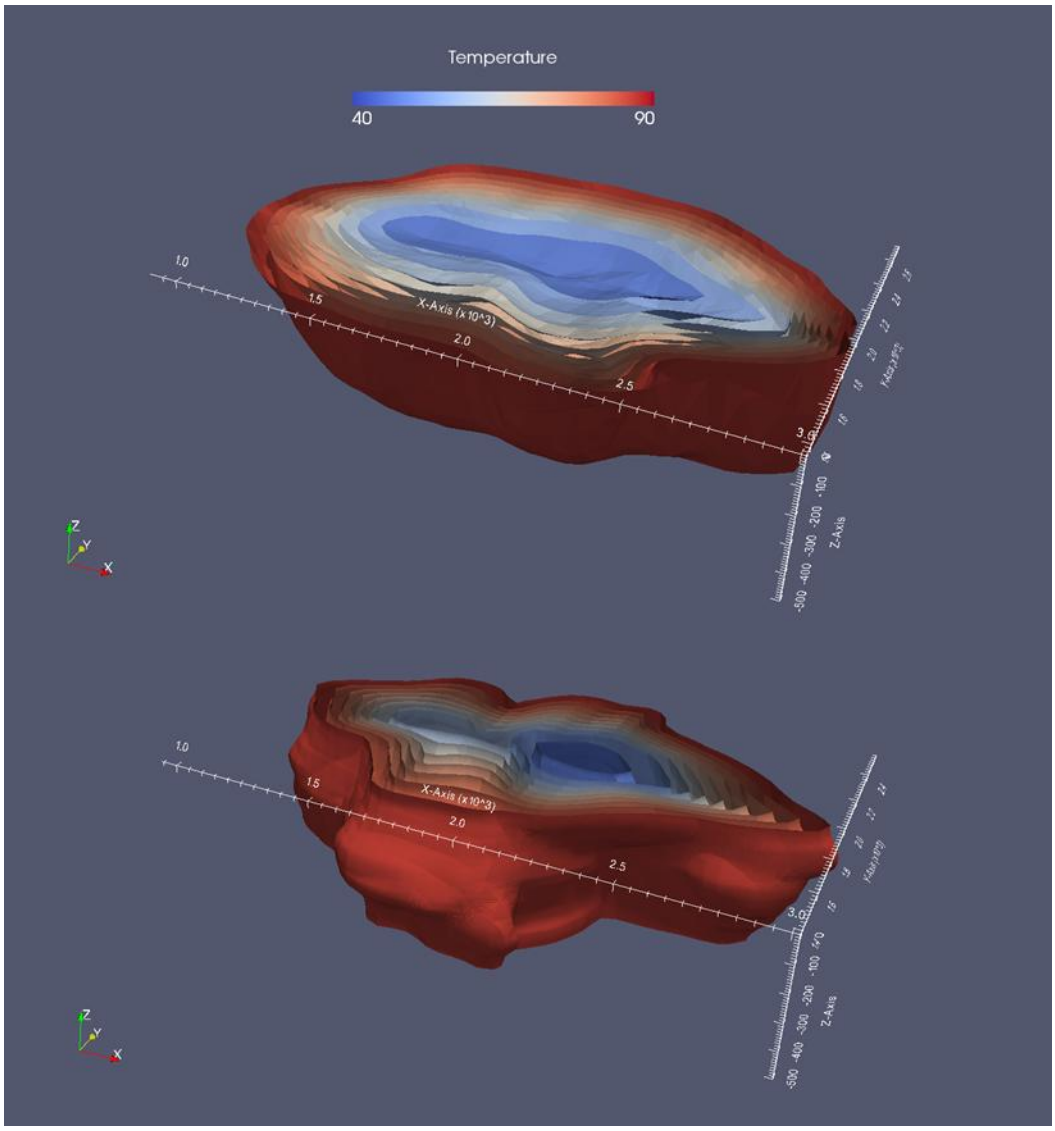

Figure 28: Comparison of the cold plume extension between the homogeneous model on the top and the heterogeneous model on the bottom. Case of horizontal wells.

CONCLUSIONS AND PERSPECTIVES

In this paper we analyzed the impact of fluvial heterogeneities on the flow and heat transport induced by geothermal exploitation at the doublet scale. We used a 3D numerical block representing realistic fluvial sedimentary heterogeneities as they are supposed to be found in the Triassic clastic series of the Paris basin. The methodology of our work consisted, firstly, to quantify the impact of these heterogeneities according to the mode of operation (vertical or horizontal wells), then to compare the development of the cold front with a conservative tracer plume, and finally to test if the vertical heterogeneities could be replaced by a simpler model.

The simulations show that in such environment, horizontal wells are particularly well adapted with a more gradual temperature decline at the production well. Moreover, when drilling horizontal wells perpendicular to the high conductive paths, the production fluid temperature is still not affected by the cold injection after 30 years of geothermal exploitation. If these results are confirmed at an experimental stage, it would be a promising breakthrough for further development in geothermal well design.

Furthermore, compared to a tracer injection which "marks" the flow paths, the volume of the reservoir impacted by the cold injection is smaller and less impacted by sedimentary heterogeneities. Following these simulation results, we tested a two-layer model

that cumulates high permeable cells in the heterogeneous model in one layer (net pay) and low permeable cells in a second layer (interstrata). The horizontal heterogeneous structure was unchanged. This attempt of simplifying the vertical structure of the heterogeneous 3D block failed in fitting temperature decline as observed in the heterogeneous model. Further study need to be done to better understand the impact of connectivity on heat transport, and to develop a method that could substitute complex sedimentary heterogeneous block by a simpler approach giving similar results.

ACKNOWLEDGMENTS

This study is part of the CLASTIQ-2 project co-funded by BRGM and the French Environment and Energy Management Agency (ADEME). We thank the ADEME for its financial support that permitted to achieve this work.

The authors are also grateful to Mines Paristech who courteously gave them the 3D numerical block produced with the Flumy software.

REFERENCES

Chilès J., Delfiner P. (1999), *Geostatistics: Modeling spatial uncertainty.* Wiley. 720 p.

Eschard R., Lemouzy P., Bacchiana C. et al. (1998), "Combining sequence stratigraphy, geostatistical simulations, and production data for modeling a fluvial reservoir in the Chaunoy field (Triassic, France)". *AAPG Bulletin*, 82, 4 p. 545-568.

Le Loc'h G. (1987), Étude de la composition des perméabilités par des méthodes variationnelles. Thèse de doctorat. Ecole Nationale Supérieure des Mines de Paris.

Lopez S. (2003), Modélisation de réservoirs chenalisés méandriformes: approche génétique et stochastique. Thèse de Docteur en Géostatistique. Ecole Nationale Supérieure des Mines de Paris.

Lopez S., Cojan I., Rivoirard J. et al. (2008), "Process-based stochastic modeling; meandering channelized reservoirs." In : Analogue and numerical modeling of sedimentary systems; from understanding to prediction. *Special Publication of the International Association of Sedimentologists*, 40, p.139-144. Ed. by Poppe de Boer, et al. Oxford : Blackwell, Oxford.

Lopez, S., Hamm, V., Le Brun, M., Schaper, L., Boissier, F., Cotiche, C., Giuglaris, E. (2010). "40 years of Dogger aquifer management in Ile-de-France, Paris Basin, France". *Geothermics*, 39, 4, p. 339-356, December 2010.

De Marsily, G. (1986). *Quantitative Hydrogeology. Groundwater Hydrology of Engineers.* Academic Press, 440 p.

Pranter M. J., Ellison A. I., Cole R. D. et al. (2007), "Analysis and modeling of intermediate-scale reservoir heterogeneity based on a fluvial point-bar outcrop analog, Williams Fork Formation, Piceance Basin, Colorado." *AAPG Bulletin*, 91, 7 p. 1025-1051.

Renard P., Le Loc'h G., Ledoux E. et al. (2000), "A fast algorithm for the estimation of the equivalent hydraulic conductivity of heterogeneous media." *Water Resources Research*, 36, 12 p. 3567-3580.

Thiéry D. (1990), MARTHE Software. Modeling of Aquifers with a Rectangular grid in Transient state for Hydrodynamic calculations of heads and flows. Release 4.3.BRGM report 4S/EAU no R32548. .

Ungemach P., Antics M., Lalos P., Borozdina O., Foulquier L., Papachristou M. (2011), "Geomodelling and well architecture, key issues to sustainable reservoir development" proceedings of the 36th Workshop on Geothermal Reservoir Engineering, Stanford University, Stanford, California, January 31 - February 2, 2011